ACS Sustainable Chemistry & Engineering

pubs.acs.org/journal/ascecg

Research Article

Bowl-like C@MoS_2 Nanocomposites as Anode Materials for Lithium-Ion Batteries: Enhanced Stress Buffering and Charge/Mass Transfer

Xiue Zhang, Xing Chen, Huajuan Ren, Guowang Diao, Ming Chen,* and Shaowei Chen*

Cite This: *ACS Sustainable Chem. Eng.* 2020, 8, 10065−10072

Read Online

ACCESS | Metrics & More | Article Recommendations | Supporting Information

ABSTRACT: Fabrication of stress-buffered nanostructured electrodes with good mechanical stability and electrical conductivity remains a daunting challenge. Herein, we describe the design and preparation of bowl-like hybrids whereby ultrathin MoS_2 nanosheets are anchored on the surfaces of mesoporous hollow carbon bowls (MHCBs). The porous bowl-like structure not only buffers mechanical stress arising from volumetric variation during the charge/discharge process but also increases the packing density of electrode materials by stacking up the carbon bowls. The resulting bowl-like C@MoS_2 hybrid structure exhibits a reversible capacity of 798 mA h g^{-1} at 0.1 A g^{-1} and outstanding long-term stability at 526 mA h g^{-1} after 1000 cycles at 1 A g^{-1}. Kinetics investigation demonstrates that the Li^+ storage is governed by the pseudocapacitive mechanism due to the porous, conductive network of MHCBs.

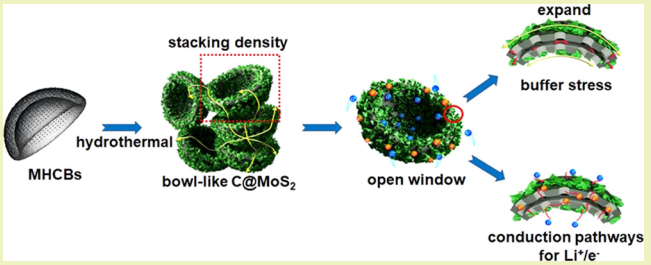

KEYWORDS: *mesoporous hollow carbon bowl, ultrathin MoS_2 nanosheets, buffer stress, cycling stability, lithium-ion battery*

INTRODUCTION

Recently, hollow spherical micro/nanostructures have received extensive attention in the field of energy storage, largely because of the high contact area between the electrolyte and electrode and the unique characteristics of buffering volumetric change of the electrode.[1−4] Notwithstanding many merits, a common drawback remains, where the large empty space within the hollow nanostructures leads to a low packing density of active materials.[5−10] Such an issue can be mitigated by having porous, bowl-like structures for the electrode materials, which cannot only buffer mechanical stress associated with volumetric changes during the discharge/discharge process to maintain the stability of the electrode but also stack up to form a favorable conductive pathway for ion transport.[11−14]

Molybdenum disulfide (MoS_2) represents a unique active material because of its high specific capacity and remarkable electrochemical activity;[15−18] however, its disadvantages, namely, poor conductivity and significant volumetric expansion during reaction with Li^+ ions, should not be overlooked from the prospective of practical battery design.[19−22] Within this context, preparation of MoS_2 and carbon nanocomposites represents an effective strategy to mitigate these issues.[5,23−27] Different MoS_2-carbon nanocomposites have been constructed for lithium-ion batteries, such as yolk−shell MoS_2@C microspheres,[28,29] core−shell C@MoS_2 microspheres,[30,31] three-dimensional MoS_2/carbon sandwiched architecture,[5] MoS_2@C nanotubes,[32,33] hierarchical MoS_2/polyaniline nanowires,[17] and MoS_2-coated three-dimensional graphene networks.[34] Among them, Wu et al.[5] sandwiched ultrathin MoS_2 nanosheets between hollow polypyrrole-derived carbon nanotubes and thin carbon layers and observed an enhanced lithium storage performance. Nevertheless, design and fabrication of a structure that can effectively reduce stress accumulation of MoS_2 remain a significant challenge, which can be achieved by using mesoporous hollow carbon bowls (MHCBs) as the structural scaffolds. This is the primary motivation of the present study.

MHCBs exhibit a unique hemispherical shape, high specific surface area, and porous structure.[35−37] Such an open structure can be exploited for buffering mechanical stress and for stacking of active materials.[38−42] For instance, Zhang et al.[39] simulated the von Mises stress distributions of carbon in four three-dimensional models under an isotropic initial stress by the finite element method and observed marked strain relaxation with the structure of a hollow multihole bowl.

Herein, we report the design and preparation of bowl-like hybrid structures whereby ultrathin MoS_2 nanosheets are anchored on the surface of MHCBs via a facile hydrothermal method, forming bowl-like C@MoS_2 nanocomposites. Such a unique architecture effectively reduces stress accumulation of

Received: March 5, 2020
Revised: June 2, 2020
Published: June 12, 2020

https://dx.doi.org/10.1021/acssuschemeng.0c01835
ACS Sustainable Chem. Eng. 2020, 8, 10065−10072

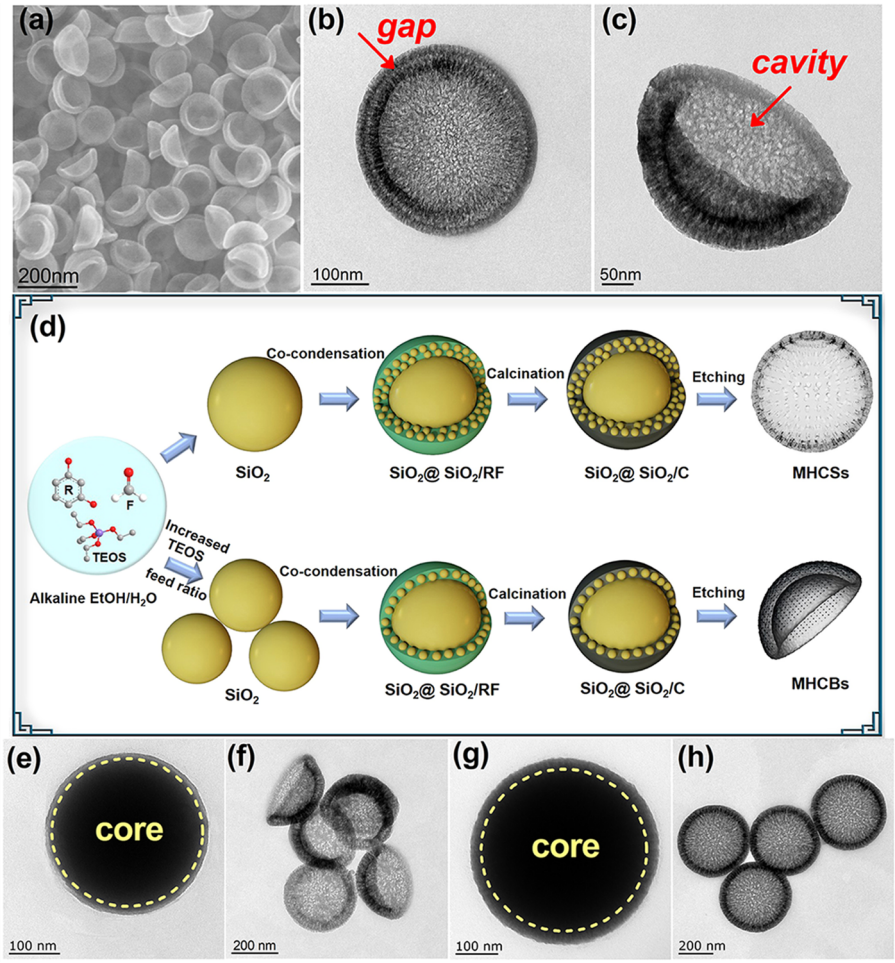

Figure 1. (a) SEM and (b, c) TEM images of carbon bowls. (d) Schematic of the preparation MHCBs and MHCSs. TEM images of the SiO_2@ SiO_2/C intermediate for (e) MHCBs and (g) MHCSs. TEM images of (f) MHCBs and (h) MHCSs.

MoS_2 and maintains the stability of the electrode, leading to a low ion-transport resistance and hence a significant increase in pseudocapacitive contribution to Li^+-ion storage. Meanwhile, it also increases the packing density of electrode materials.

EXPERIMENTAL SECTION

Synthesis of Mesoporous Hollow Carbon Bowls (MHCBs). To prepare MHCBs, ammonia (4.5 mL), tetraethyl orthosilicate (TEOS, 8.6 mL), resorcinol (0.6 g), and formaldehyde (0.84 mL) were added to the mixture of ethanol (100 mL) and deionized water (15 mL) under heat and magnetic stirring. The resultant product of SiO_2@SiO_2/RF (resorcinol-formaldehyde) composites was then dried and carbonized under N_2 at 700 °C for 4 h. MHCBs were acquired after the removal of silica by using NaOH solution at 80 °C.

Mesoporous hollow carbon spheres (MHCSs) were prepared in a similar fashion but at a reduced TEOS feed ratio (the dosages of TEOS/resorcinol/formaldehyde were 3.46 mL/0.4 g/0.56 mL).

Synthesis of Bowl-like C@MoS_2 Composites. $(NH_4)_2MoS_4$ powder (0.25 g) was dispersed in 10 mL of dimethylformamide (DMF) under ultrasonication, into which was then added the MHCBs (0.05 g) prepared above under vigorous stirring for 30 min before the addition of 0.1 mL of $(NH_2)_2{\cdot}H_2O$. The mixture was heated at 180 °C for 5 h in a Teflon-lined autoclave (50 mL). The resultant solid was collected and washed. Last, the solid was calcined under a N_2 atmosphere at 850 °C for 4 h. The synthesized black powder was C@MoS_2 nanobowls.

Pure MoS_2 was also prepared in the same fashion but without the addition of MHCBs.

Characterization. The samples were characterized using a Supra 55 scanning electron microscope (SEM, Supra 55 VP, 5.0 kV), transmission electron microscope (TEM, Tecnai 12, 200 kV), and high-resolution TEM (HRTEM, Tecnai G2 F30 S-TWIN, 300 kV). X-ray powder diffraction (XRD) data were measured using a D8 advance superspeed powder diffractometer (Bruker), and Raman analysis was conducted with an InVia Raman microscope (Renishaw, incident laser wavelength λ = 532 nm). Surface chemical species were examined by X-ray photoelectron spectroscopy (XPS, Escalab250Xi). Thermogravimetric analysis (TGA) was carried out with a PerkinElmer Pyris 1 analyzer. Nitrogen adsorption−desorption isotherms were collected with an ASAP 2020 HD88 instrument.

Electrochemical Test. The electrochemical tests were evaluated by cycling a two-electrode CR 2032 coin-type cell with lithium foil as the reference and counter electrodes and a polypropylene film (Celgard 2400) as the separator, and the working electrodes were manufactured by mixing the bowl-like C@MoS_2 (80 wt %), Super P (10 wt %), and polyvinylidene difluoride (PVDF, 10 wt %) on the copper foil. The electrode had a diameter of 16 mm and a loading density of 2 mg cm^{-2}. $LiPF_6$ (1 mol L^{-1}) was mixed with EC/DEC/EMC by a volume ratio of 1:1:1 as the electrolyte. The half-battery performance test was implemented on a Xinwei CT-3008 W battery test system. Cyclic voltammetry (CV) was conducted using a CHI 660E electrochemical workstation. Nyquist plots were conducted on a Biologic VMP3 electrochemical workstation.

RESULTS AND DISCUSSION

From the SEM image in Figure 1a, one can see that the MHCBs are uniformly dispersed with a clear bowl-shaped

https://dx.doi.org/10.1021/acssuschemeng.0c01835
ACS Sustainable Chem. Eng. 2020, 8, 10065−10072

structure. TEM analysis of upended MHCBs clearly shows that the bowl wall consists of two shells (each ca. 17 nm in thickness and separated by a gap of ca. 5 nm) with a bowl diameter of ca. 320 nm (Figure 1b,c).[19,43] Nitrogen adsorption−desorption measurements (Figure S1) confirmed the mesoporosity of the MHCBs, which displayed a specific surface area of 873.4 $m^2 g^{-1}$ and a pore diameter mostly at 3.1 nm. The formation of carbon nanobowls likely entails the following steps (Figure 1d): (i) hydrolysis of TEOS led to formation of SiO_2 nanospheres; (ii) co-condensation polymerization of TEOS and RF precursors produced a SiO_2/RF shell on the SiO_2 nanosphere surface (SiO_2@SiO_2/RF, Figure S2a,b); (iii) controlled pyrolysis of SiO_2@SiO_2/RF led to effective carbonization of the RF shell (SiO_2@SiO_2/C, Figure 1e and Figure S2c,d); and (iv) upon removal of SiO_2 by NaOH etching at 80 °C, the thin mesoporous carbon shell did not have sufficient mechanical strength to support the hollow carbon nanospheres and collapsed into porous nanobowls (Figure 1f).[35,44]

Note that when the TEOS-to-RF feed ratio is decreased, pyrolysis of the obtained SiO_2@SiO_2/RF intermediate produced a SiO_2@SiO_2/C core@shell structure with a thicker carbon shell (Figure 1g and Figure S3a,b). After NaOH etching of the SiO_2 core, the relatively thick carbon shell retained the spherical shell to form the mesoporous hollow carbon spheres (MHCSs) (Figure 1h and Figure S3c). The MHCSs exhibit specific surface areas of 770.7 $m^2 g^{-1}$, with the diameters of most pores of 2.1 nm (Figure S4).

A second hydrothermal treatment was then carried out to in situ grow ultrathin MoS_2 nanosheets on MHCB surfaces, forming bowl-like C@MoS_2 composites (Figure 2a). From Figure 2b−d, one can see that the C@MoS_2 nanocomposites largely retain the bowl-like morphology of MHCBs but with a markedly roughened surface and a slight increase in diameter to 330 nm. Note that the nanobowls can stack up through the bowl opening (Figure S5). Such stacking may increase the tap density and bulk density, and the interconnected channels can facilitate ion transport, an important feature for charge storage.[12,45−47] From HRTEM measurements (Figure 2e), it can be seen that the MHCBs are intimately encapsulated by few-layered MoS_2 nanosheets (two to six layers, Figure 2e1), which exhibit an interplanar spacing of ca. 0.63 nm (Figure 2f). This is slightly larger than that of pure MoS_2 (0.62 nm), corresponding to the (002) planes of hexagonal MoS_2 (Figure 2g).[18] In elemental mapping analysis based on EDX measurements (Figure 2h−l), the elements of C, Mo, and S can be found to be evenly distributed within the sample, confirming the uniform dispersion of MoS_2 and C in the bowl-like C@MoS_2 hybrid structure. Furthermore, TGA measurements show that the MoS_2 content in bowl-like C@MoS_2 is about 81 wt % (Figure S6).

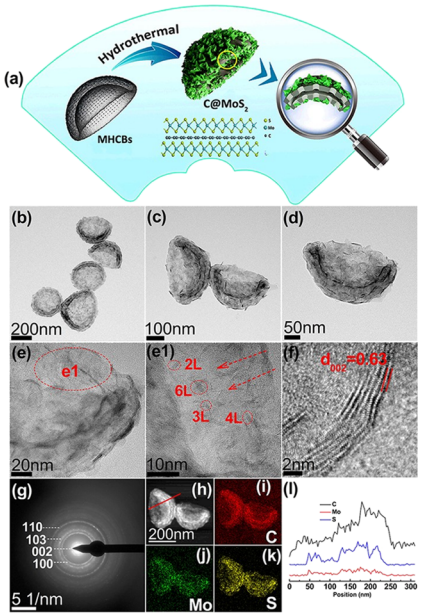

Figure 2. (a) Schematic procedure for the formation of bowl-like C@MoS_2 nanocomposites. (b−d) TEM images, (e, e1, f) HRTEM images, (g) SAED patterns, (h−k) annular dark-field STEM image and the corresponding EDX elemental mappings of C, Mo, and S, and (l) EDX line-scan profiles of C@MoS_2 composites (red line in panel h).

Further structural insights were obtained by XRD measurements (Figure 3a). For pure MoS_2 (which was prepared by the same hydrothermal method but in the absence of the MHCBs, Figure S7) and bowl-like C@MoS_2, four major peaks can be identified at 2θ = 14.2, 32.9, 39.5, and 58.3°, which can be indexed to the (002), (100), (103), and (110) diffractions of hexagonal MoS_2 (JCPDS card no. 37-1492), respectively.[18,19,48] In Raman measurements (Figure 3b), the MoS_2 A_{1g} and E^1_{2g} vibrations can be identified at 404 and 377 cm^{-1}, respectively, for both pristine MoS_2 and bowl-like C@MoS_2 samples; the latter shows two additional vibrations at 1336 and 1597 cm^{-1} due to the two characteristic peaks of graphitic carbon, i.e., D and G bands, further confirming the formation of MoS_2 and carbon nanocomposites.[49] From the nitrogen adsorption−desorption isotherm in Figure 3c, the specific surface area of bowl-like C@MoS_2 is estimated to be 141.9 $m^2 g^{-1}$, with the pores mostly at 2.6 and 3.8 nm (Figure 3c inset). The fact that the specific surface area of C@MoS_2 is markedly lower than that of the MHCBs (Figure S1) is consistent with the growth of MoS_2 layer onto the carbon shell surface.

The chemical composition and valence state of the samples were then quantified by XPS measurements. Figure 3d shows the high-resolution C 1s spectrum of bowl-like C@MoS_2, where deconvolution yields three components, C−C (284.0 eV), C−O (285.4 eV), and C═O (287.6 eV).[50,51] Likewise, the Mo 3d spectrum (Figure 3e) can be found to mainly entail a doublet at 228.5 eV (Mo $3d_{5/2}$) and 231.7 eV (Mo $3d_{3/2}$) that is characteristic of Mo^{4+} and an additional peak at 234.6 eV for Mo−O due to the surface oxidation of MoS_2.[52−56] The corresponding S 2p spectrum is shown in Figure 3f, where the S $2p_{1/2}$ and S $2p_{3/2}$ electrons can be resolved at 162.6 and 161.4 eV, respectively.[51]

The obtained bowl-like C@MoS_2 nanocomposites were then examined for Li^+-ion storage. Figure 4a,b depicts the first three cyclic voltammetric (CV) scans of the bowl-like C@MoS_2 and pristine MoS_2 electrode in 0.005−3 V at a scan rate of 0.1 mV s^{-1}. Figure 4a shows that the CV profiles of C@MoS_2 reached a steady state after the first cycle. In the first scan, the cathodic peak at 1.1 V can be ascribed to the formation of Li_xMoS_2 by the Li^+ intercalation into the MoS_2 lattice[19,57] and the one at 0.5 V to the conversion reaction to form Mo nanoparticles embedded in Li_2S. Upon the reverse scan, the inconspicuous peak at around 1.7 V can be attributed to the partial oxidation of Mo, while that at 2.3 V corresponds to the oxidation of Li_2S to sulfur.[50] In the subsequent CV cycles, the second and third cycles showed an apparent

https://dx.doi.org/10.1021/acssuschemeng.0c01835
ACS Sustainable Chem. Eng. 2020, 8, 10065−10072

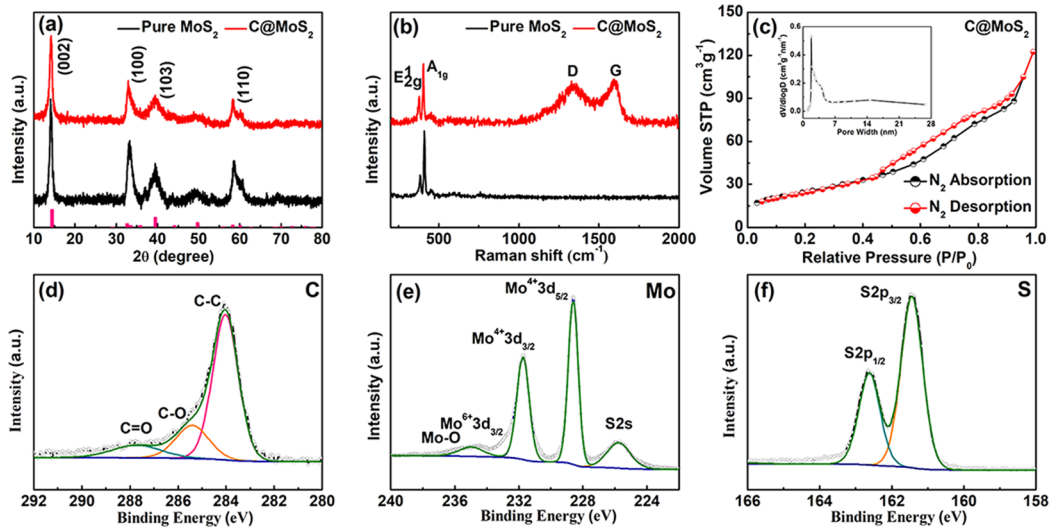

Figure 3. (a) XRD patterns and (b) Raman spectra of bowl-like C@MoS_2 and pure MoS_2 nanosheets. (c) BET nitrogen adsorption and desorption isotherms. The inset is the pore size distribution. High-resolution XPS scans of (d) C 1s, (e) Mo 3d, and (f) S 2p electrons of the bowl-like C@MoS_2 nanocomposites.

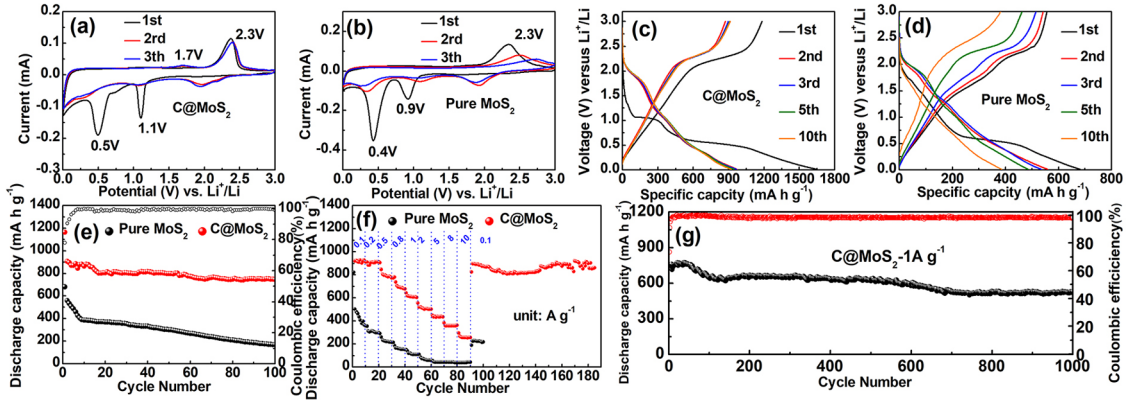

Figure 4. Electrochemical performances of bowl-like C@MoS_2 and pure MoS_2 nanosheets as anode materials for LIBs: (a, b) CV profiles over a voltage range of 0.005−3.0 V at a scan rate of 0.1 mV s^{-1}; (c, d) charge/discharge profiles at 0.1 A g^{-1}; (e) cycling performance at 0.1 A g^{-1}; (f) rate performances; and (g) cycling performance of bowl-like C@MoS_2 at 1 A g^{-1}.

overlap, but the current density decreased somewhat as compared to the first cycle. By contrast, whereas pure MoS_2 (Figure 4b) exhibits similar CV profiles, the current densities are markedly lower, and the unstable CV profiles demonstrate poor stability of pure MoS_2. This suggests the significance of the carbon bowl frame in the accommodation of the volumetric changes during Li^+ charge and discharge.[58]

The first discharge and charge steps of the bowl-like C@MoS_2 and pure MoS_2 electrodes at 0.1 A g^{-1} are shown in Figure 4c,d. The bowl-like C@MoS_2 electrode exhibits an initial discharge/charge capacity of 1516/1183 mA h g^{-1} at 0.1 A g^{-1} with an initial coulombic efficiency of 78% (Figure 4c). In comparison, the discharge/charge capacity of pure MoS_2 is about 50% lower at 859/556 mA h g^{-1} at the same current density (Figure 4d). The few-layered nanosheets (two to six layers) and the enlargement of interlayer spacing of MoS_2 in bowl-like C@MoS_2 improve the reversibility of the Li^+ intercalation/extraction reaction, which increases the initial coulombic efficiency. After 100 cycles, the specific capacity of the bowl-like C@MoS_2 electrode is stabilized at 798 mA h g^{-1} at 0.1 A g^{-1}, which is 82% of the second-cycle discharge capacity (970 mA h g^{-1}). It is a remarkable fact that carbon bowls also contributed a small amount of capacity (Figure S8). In contrast, the pure MoS_2 showed severe capacity decay and eventually almost failed (Figure 4e). The rate capability of both electrodes was then tested at current densities from 0.1 to 10 A g^{-1} (Figure 4f). The reversible discharge capacities of bowl-like C@MoS_2 are 922 mA h g^{-1} at 0.1 A g^{-1} and 256 mA h g^{-1} at 10 A g^{-1}. Notably, the bowl-like C@MoS_2 electrode retained an initial specific capacity of 897 mA h g^{-1} after 100 cycles from 10 to 0.1 A g^{-1}. The good rate performance is mainly attributed to the bowl-shaped stacking structure of C@MoS_2, which shortened the electron/ion transport distance.

Figure 4g exhibits the long-term cycle stability of bowl-like C@MoS_2. Even at 1 A g^{-1}, bowl-like C@MoS_2 delivers a capacity as high as 526 mA h g^{-1} after 1000 cycles, with a retention of 70%. TEM measurements show no apparent variation of the structural morphologies (Figure S9). For comparison, pure MoS_2 shows poor cycle life with a low capacity of 166 mA h g^{-1} after 100 cycles at 0.1 A g^{-1}. In fact, the bowl-like C@MoS_2 exhibits much better long-term cycling performance than results reported in recent literature with relevant MoS_2-based materials (Table S1). The long cycle stability of the C@MoS_2 electrode at high current densities

https://dx.doi.org/10.1021/acssuschemeng.0c01835
ACS Sustainable Chem. Eng. 2020, 8, 10065−10072

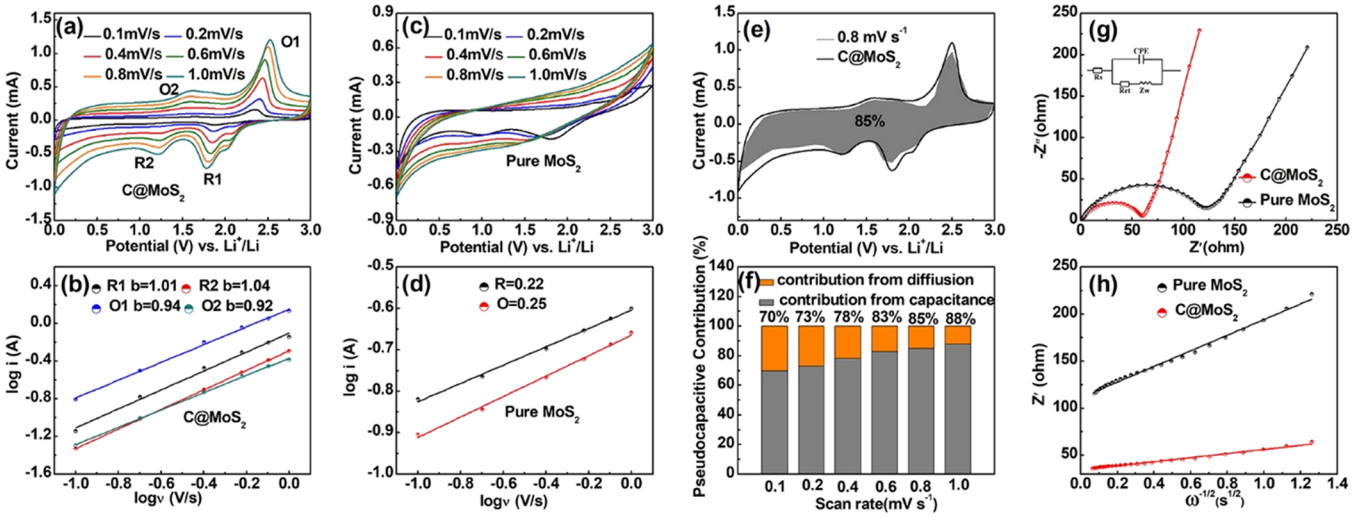

Figure 5. (a) CV curves of bowl-like C@MoS_2 at different scan rates. (b) log i versus log v plot at different oxidation and reduction states. (c) CV curves of pure MoS_2 at different scan rates. (d) log i versus log v plot at different oxidation and reduction states. (e) Capacitive contribution at 0.8 mV s^{-1}. (f) Capacitive contribution ratio at various sweep rates. (g) Nyquist plots and equivalent circuit model (inset) and (h) the variation of Z' versus $\omega^{-1/2}$ in the low frequency region for C@MoS_2 and pure MoS_2.

may be ascribed to the porous, bowl-like structure that facilitates Li^+/ion transport and buffering of mechanical stress during the change/discharge process.[11,12,59]

Notably, the shape of the CV curves of the bowl-like C@MoS_2 electrode is well preserved with the scan rate increased from 0.1 to 1.0 mV s^{-1} (Figure 5a), in contrast to that of pure MoS_2 (Figure 5c). According to equations[60,61]

$$i = a\nu^b \tag{1}$$

$$\log i = \log a + b\log \nu \tag{2}$$

where i is the current density, ν is the potential scan rate, and a and b are constants. If $b \approx 0.5$, the electrochemical reaction is predominated by a diffusion-controlled process; at $b \approx 1$, it is dominated by a capacitive process. From the linear regression of the experimental data (Figure 5b), the calculated b values for four peaks (R1, R2, O1, O2) are 1.01, 1.04, 0.94, and 0.92, respectively, suggesting the pseudocapacitive dominant characteristic. The few-layered ultrathin MoS_2 nanosheets (two to six layers, Figure 2e1) and the large specific surface area (141.9 m^2 g^{-1}) of bowl-like C@MoS_2 reduce the diffusion path of the ions and prompt the lithium storage reaction mainly occurring on the surface of nanosheets. The b values of pure MoS_2 are only 0.22 and 0.25 (Figure 5d). One can see that the b values of bowl-like C@MoS_2 are apparently higher than those of pure MoS_2. This is likely because the incorporation of the carbon bowls is effective in the conversion of the electrochemical process from the diffusion behavior to capacitive process, leading to the rapid Li-ion intercalation/extraction reaction.

Furthermore, the pseudocapacitive contribution can be calculated from the following equations:[62]

$$i = k_1\nu + k_2\nu^{1/2} \tag{3}$$

$$i/\nu^{1/2} = k_1\nu^{1/2} + k_2 \tag{4}$$

where i is the current at a particular potential, ν is the potential scan rate, and k_1 and k_2 are variable parameters. Figure 5e shows the pseudocapacitive fraction (gray area) of bowl-like C@MoS_2 at a scan rate of 0.8 mV s^{-1}, which is drastically higher than that of pure MoS_2 (41%, Figure S10). The capacitive contribution is enhanced gradually with the increase in potential sweep rate (Figure 5f). This may be, at least in part, ascribed to the conductive carbon bowls that improve the reactivity and buffer the mechanic stress of MoS_2.[47,63] In addition, the EIS measurements were conducted in the frequency range 10−0.01 Hz at 5 mV amplitude on the fresh cells. Electrochemical impedance measurements show that the charge-transfer resistance (R_{ct}) of bowl-like C@MoS_2 (59 Ω) is markedly lower than that of pure MoS_2 (122 Ω) (Figure 5g), further confirming the enhanced electron/ionic conductivity of the bowl-like C@MoS_2. In addition, the linear segment in the low-frequency regime can be seen to show a lower slope with bowl-like C@MoS_2 than with pure MoS_2 (Figure 5h and Table S2), suggesting enhanced Li^+-ion diffusion through the electrode.[43,64]

The stable cycle life and high-rate performance of C@MoS_2 observed above can be ascribed to the unique bowl-like structure (Figure 6). (1) Stacking of the bowl-shaped C@MoS_2 with interconnected windows can improve the bulk density and shorten transport path of ions. (2) The bowl-like C@MoS_2 with open windows can increase the contact area between Li^+/ion and electrolytes. (3) The carbon bowl frameworks can effectively relieve stress of MoS_2 nanosheets to prevent exfoliation and maintain the structural integrity of the electrode material. (4) The ultrathin MoS_2 nanosheets anchored on mesoporous carbon bowls can offer effective

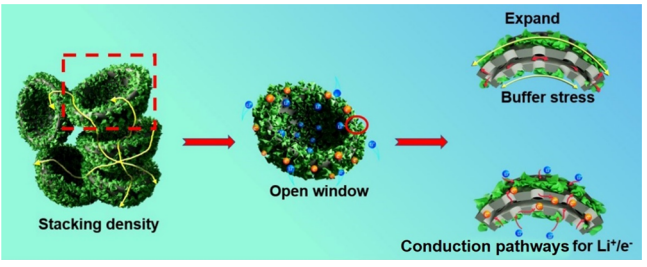

Figure 6. Schematic diagram of the structure advantages of the bowl-like C@MoS_2.

https://dx.doi.org/10.1021/acssuschemeng.0c01835
ACS Sustainable Chem. Eng. 2020, 8, 10065−10072

pathways for Li^+/ion, leading to reduced ion-transport resistance, easy penetration by the electrolyte ions into the bowl-like framework, and ultimately improved lithium-ion kinetics.

CONCLUSIONS

Bowl-like C@MoS_2 nanocomposites were prepared by the growth of few-layered MoS_2 nanosheets onto the carbon bowl surface. The porous framework effectively buffered the mechanical stress caused by the volumetric changes of MoS_2 nanosheets during the insertion/delithium process, thereby sustaining the structural integrity of the electrode. The bowl-like C@MoS_2 exhibited excellent rate capability and cycling stability due to the carbon bowl framework with open windows and interconnected channels that facilitated efficient electron and ion transport. The electrochemical kinetics study showed that the pseudocapacitive mechanism dominated the energy storage process. Moreover, the local stacking behavior of the bowl-like C@MoS_2 provided a unique strategy for an increased bulk density. Results from this study highlight the significance of functional nanostructured materials in the design and engineering of high-performance anodes for lithium-ion batteries.

ASSOCIATED CONTENT

Supporting Information

The Supporting Information is available free of charge at https://pubs.acs.org/doi/10.1021/acssuschemeng.0c01835.

N_2 adsorption and desorption and pore size distribution of MHCBs and MHCSs, SEM and TEM images of SiO_2@SiO_2/RF nanospheres and SiO_2@SiO_2/C nanospheres for the preparation of MHCBs, SEM and TEM images of SiO_2@SiO_2/C nanospheres and the mesoporous hollow carbon spheres (MHCSs), SEM images of bowl-like C@MoS_2, TGA curves of pure MoS_2 and bowl-like C@MoS_2, SEM images and TEM images of pure MoS_2, rate performance comparison of MHCBs, cycling performances of MHCBs at 1 A g^{-1}, TEM images of the bowl-like C@MoS_2 after cycling, capacitive contribution at 0.8 mV s^{-1} of pure MoS_2, the performances of the reported MoS_2-based materials for LIBs, and EIS parameters (PDF)

AUTHOR INFORMATION

Corresponding Authors

Ming Chen − *School of Chemistry and Chemical Engineering, Yangzhou University, Yangzhou 225002, P. R. China; Key Laboratory of Advanced Energy Materials Chemistry (Ministry of Education), College of Chemistry, Nankai University, Tianjin 300071, P. R. China;* orcid.org/0000-0002-6436-4765; Email: chenming@yzu.edu.cn

Shaowei Chen − *Department of Chemistry and Biochemistry, University of California, Santa Cruz, California 95064, United States;* orcid.org/0000-0002-3668-8551; Email: shaowei@ucsc.edu

Authors

Xiue Zhang − *School of Chemistry and Chemical Engineering, Yangzhou University, Yangzhou 225002, P. R. China; Department of Chemistry and Biochemistry, University of California, Santa Cruz, California 95064, United States*

Xing Chen − *School of Chemistry and Chemical Engineering, Yangzhou University, Yangzhou 225002, P. R. China*

Huajuan Ren − *School of Chemistry and Chemical Engineering, Yangzhou University, Yangzhou 225002, P. R. China*

Guowang Diao − *School of Chemistry and Chemical Engineering, Yangzhou University, Yangzhou 225002, P. R. China*

Complete contact information is available at: https://pubs.acs.org/10.1021/acssuschemeng.0c01835

Notes

The authors declare no competing financial interest.

ACKNOWLEDGMENTS

This work was supported by the National Natural Science Foundation of China (grant no. 21773203), the Yangzhou University International Academic Exchange Fund (YZUIAEF201901003), and the Program for Priority Academic Development of Jiangsu Higher Education Institutions. S.C. acknowledges partial support from the National Science Foundation (CBET-1848841 and CHE-1900235).

REFERENCES

(1) Wang, X.; Feng, J.; Bai, Y.; Zhang, Q.; Yin, Y. Synthesis, Properties, and Applications of Hollow Micro-/Nanostructures. *Chem. Rev.* **2016**, *116*, 10983−11060.

(2) Liu, J.; Qiao, S. Z.; Chen, J. S.; Lou, X. W. D.; Xing, X.; Lu, G. Q. M. Yolk/shell nanoparticles: new platforms for nanoreactors, drug delivery and lithium-ion batteries. *Chem. Commun.* **2011**, *47*, 12578−12591.

(3) Zhou, L.; Zhang, K.; Hu, Z.; Tao, Z.; Mai, L.; Kang, Y.-M.; Chou, S.-L.; Chen, J. Recent Developments on and Prospects for Electrode Materials with Hierarchical Structures for Lithium-Ion Batteries. *Adv. Energy Mater.* **2018**, *8*, 1701415.

(4) Zhang, S.; Zheng, Y.; Huang, X.; Hong, J.; Cao, B.; Hao, J.; Fan, Q.; Zhou, T.; Guo, Z. Structural Engineering of Hierarchical Micro-nanostructured Ge−C Framework by Controlling the Nucleation for Ultralong-Life Li Storage. *Adv. Energy Mater.* **2019**, *9*, 1900081.

(5) Wu, C.; Ou, J. Z.; He, F.; Ding, J.; Luo, W.; Wu, M.; Zhang, H. Three-dimensional MoS_2/Carbon sandwiched architecture for boosted lithium storage capability. *Nano Energy* **2019**, *65*, 104061.

(6) Zhou, L.; Zhao, D.; Lou, X. D. LiNi0.5Mn1.5O4 hollow structures as high-performance cathodes for lithium-ion batteries. *Angew. Chem., Int. Ed.* **2012**, *51*, 239−241.

(7) Yue, Q.; Jiang, H.; Hu, Y.; Jia, G.; Li, C. Mesoporous single-crystalline V_2O_5 nanorods assembled into hollow microspheres as cathode materials for high-rate and long-life lithium-ion batteries. *Chem. Commun.* **2014**, *50*, 13362−13365.

(8) Wu, Z.; Wang, W.; Wang, Y.; Chen, C.; Li, K.; Zhao, G.; Sun, C.; Chen, W.; Ni, L.; Diao, G. Three-dimensional graphene hollow spheres with high sulfur loading for high-performance lithium-sulfur batteries. *Electrochim. Acta* **2017**, *224*, 527−533.

(9) Han, J.; Chen, R.; Wang, M.; Lu, S.; Guo, R. Core-shell to yolk-shell nanostructure transformation by a novel sacrificial template-free strategy. *Chem. Commun.* **2013**, *49*, 11566−11568.

(10) Qian, C.; Guo, P.; Zhang, X.; Zhao, R.; Wu, Q.; Huan, L.; Shen, X.; Chen, M. Nitrogen-doped mesoporous hollow carbon nanoflowers as high performance anode materials of lithium ion batteries. *RSC Adv.* **2016**, *6*, 93519−93524.

(11) Liang, J.; Yu, X.-Y.; Zhou, H.; Wu, H. B.; Ding, S.; Lou, X. W. D. Bowl-like SnO_2 @carbon hollow particles as an advanced anode material for lithium-ion batteries. *Angew. Chem., Int. Ed.* **2014**, *53*, 12803−12807.

(12) Liang, J.; Hu, H.; Park, H.; Xiao, C.; Ding, S.; Paik, U.; Lou, X. W. D. Construction of hybrid bowl-like structures by anchoring NiO

nanosheets on flat carbon hollow particles with enhanced lithium storage properties. *Energy Environ. Sci.* **2015**, *8*, 1707−1711.
(13) Vu, A.; Qian, Y.; Stein, A. Porous Electrode Materials for Lithium-Ion Batteries - How to Prepare Them and What Makes Them Special. *Adv. Energy Mater.* **2012**, *2*, 1056−1085.
(14) Wang, J.; Zhan, R.; Fu, Y.; Yu, H.-Y.; Jiang, C.; Zhang, T.-H.; Zhang, C.; Yao, J.; Li, J.-F.; Li, X.; Tian, J.-H.; Yang, R. Design and synthesis of hierarchical, freestanding bowl-like $NiCo_2O_4$ as cathode for long-life Li-O_2 batteries. *Mater. Today Energy* **2017**, *5*, 214−221.
(15) Yousaf, M.; Mahmood, A.; Wang, Y.; Chen, Y.; Ma, Z.; Han, R. P. S. Advancement in Layered Transition Metal Dichalcogenide Composites for Lithium and Sodium Ion Batteries. *J. Electr. Eng.* **2016**, *4*, 58−74.
(16) Pumera, M.; Sofer, Z.; Ambrosi, A. Layered transition metal dichalcogenides for electrochemical energy generation and storage. *J. Mater. Chem. A* **2014**, *2*, 8981−8987.
(17) Yang, L.; Wang, S.; Mao, J.; Deng, J.; Gao, Q.; Tang, Y.; Schmidt, O. G. Hierarchical MoS_2/polyaniline nanowires with excellent electrochemical performance for lithium-ion batteries. *Adv. Mater.* **2013**, *25*, 1180−1184.
(18) Hou, M.; Qiu, Y.; Yan, G.; Wang, J.; Zhan, D.; Liu, X.; Gao, J.; Lai, L. Aging mechanism of MoS_2 nanosheets confined in N-doped mesoporous carbon spheres for sodium-ion batteries. *Nano Energy* **2019**, *62*, 299−309.
(19) Zhang, X.; Zhao, R.; Wu, Q.; Li, W.; Shen, C.; Ni, L.; Yan, H.; Diao, G.; Chen, M. Petal-like MoS_2 Nanosheets Space-Confined in Hollow Mesoporous Carbon Spheres for Enhanced Lithium Storage Performance. *ACS Nano* **2017**, *11*, 8429−8436.
(20) Zheng, Z.; Li, P.; Huang, J.; Liu, H.; Zao, Y.; Hu, Z.; Zhang, L.; Chen, H.; Wang, M.-S.; Peng, D.-L.; Zhang, Q. High performance columnar-like Fe_2O_3@carbon composite anode via yolk@shell structural design. *J. Energy Chem.* **2020**, *41*, 126−134.
(21) Zhao, L.; Wu, H.-H.; Yang, C.; Zhang, Q.; Zhong, G.; Zheng, Z.; Chen, H.; Wang, J.; He, K.; Wang, B.; Zhu, T.; Zeng, X. C.; Liu, M.; Wang, M.-S. Mechanistic Origin of the High Performance of Yolk@Shell Bi_2S_3@N-Doped Carbon Nanowire Electrodes. *ACS Nano* **2018**, *12*, 12597−12611.
(22) Zhang, Q.; Chen, H.; Luo, L.; Zhao, B.; Luo, H.; Han, X.; Wang, J.; Wang, C.; Yang, Y.; Zhu, T.; Liu, M. Harnessing the concurrent reaction dynamics in active Si and Ge to achieve high performance lithium-ion batteries. *Energy Environ. Sci.* **2018**, *11*, 669−681.
(23) Park, S.-K.; Lee, J.; Bong, S.; Jang, B.; Seong, K.-d.; Piao, Y. Scalable Synthesis of Few-Layer MoS_2 Incorporated into Hierarchical Porous Carbon Nanosheets for High-Performance Li- and Na-Ion Battery Anodes. *ACS Appl. Mater. Interfaces* **2016**, *8*, 19456−19465.
(24) Zhang, C.-L.; Jiang, Z.-H.; Lu, B.-R.; Liu, J.-T.; Cao, F.-H.; Li, H.; Yu, Z.-L.; Yu, S.-H. MoS_2 nanoplates assembled on electrospun polyacrylonitrile-metal organic framework-derived carbon fibers for lithium storage. *Nano Energy* **2019**, *61*, 104−110.
(25) Shan, T.-T.; Xin, S.; You, Y.; Cong, H.-P.; Yu, S.-H.; Manthiram, A. Combining Nitrogen-Doped Graphene Sheets and MoS_2: A Unique Film-Foam-Film Structure for Enhanced Lithium Storage. *Angew. Chem., Int. Ed.* **2016**, *55*, 12783−12788.
(26) Naz, R.; Imtiaz, M.; Liu, Q.; Yao, L.; Abbas, W.; Li, T.; Zada, I.; Yuan, Y.; Chen, W.; Gu, J. Highly defective 1T-MoS_2 nanosheets on 3D reduced graphene oxide networks for supercapacitors. *Carbon* **2019**, *152*, 697−703.
(27) Sun, B.; Liu, Q.; Chen, W.; Wang, N.; Gu, J.; Zhang, W.; Su, H.; Zhang, D. Micron-sized encapsulated-type MoS_2/C hybrid particulates with an effective confinement effect for improving the cycling performance of LIB anodes. *J. Mater. Chem. A* **2018**, *6*, 6289−6298.
(28) Pan, Y.; Zhang, J.; Lu, H. Uniform Yolk-Shell MoS_2@Carbon Microsphere Anodes for High-Performance Lithium-Ion Batteries. *Chem. − Eur. J.* **2017**, *23*, 9937−9945.
(29) Guo, B.; Feng, Y.; Chen, X.; Li, B.; Yu, K. Preparation of yolk-shell MoS_2 nanospheres covered with carbon shell for excellent lithium-ion battery anodes. *Appl. Surf. Sci.* **2018**, *434*, 1021−1029.
(30) Wan, Z.; Shao, J.; Yun, J.; Zheng, H.; Gao, T.; Shen, M.; Qu, Q.; Zheng, H. Core-shell structure of hierarchical quasi-hollow MoS_2 microspheres encapsulated porous carbon as stable anode for Li-ion batteries. *Small* **2014**, *10*, 4975−4981.
(31) Wang, Y.; Ma, Z.; Chen, Y.; Zou, M.; Yousaf, M.; Yang, Y.; Yang, L.; Cao, A.; Han, R. P. S. Controlled Synthesis of Core-Shell Carbon@MoS_2 Nanotube Sponges as High-Performance Battery Electrodes. *Adv. Mater.* **2016**, *28*, 10175−10181.
(32) Zhang, X.; Li, X.; Liang, J.; Zhu, Y.; Qian, Y. Synthesis of MoS_2@C Nanotubes Via the Kirkendall Effect with Enhanced Electrochemical Performance for Lithium Ion and Sodium Ion Batteries. *Small* **2016**, *12*, 2484−2491.
(33) Zhu, C.; Mu, X.; van Aken, P. A.; Maier, J.; Yu, Y. Fast Li Storage in MoS_2-Graphene-Carbon Nanotube Nanocomposites: Advantageous Functional Integration of 0D, 1D, and 2D Nanostructures. *Adv. Energy Mater.* **2015**, *5*, 1401170.
(34) Cao, X.; Shi, Y.; Shi, W.; Rui, X.; Yan, Q.; Kong, J.; Zhang, H. Preparation of MoS_2-coated three-dimensional graphene networks for high-performance anode material in lithium-ion batteries. *Small* **2013**, *9*, 3433−3438.
(35) Li, S.; Pasc, A.; Fierro, V.; Celzard, A. Hollow carbon spheres, synthesis and applications − a review. *J. Mater. Chem. A* **2016**, *4*, 12686−12713.
(36) Liu, D.; Peng, X.; Wu, B.; Zheng, X.; Chuong, T. T.; Li, J.; Sun, S.; Stucky, G. D. Uniform Concave Polystyrene-Carbon Core-Shell Nanospheres by a Swelling Induced Buckling Process. *J. Am. Chem. Soc.* **2015**, *137*, 9772−9775.
(37) Fang, Y.; Lv, Y.; Gong, F.; Wu, Z.; Li, X.; Zhu, H.; Zhou, L.; Yao, C.; Zhang, F.; Zheng, G.; Zhao, D. Interface tension-induced synthesis of monodispersed mesoporous carbon hemispheres. *J. Am. Chem. Soc.* **2015**, *137*, 2808−2811.
(38) Huang, M.; Jiang, X.; Zhang, H.; Yin, H.; Li, X.; Ju, X. Bowl-like carbon sheet for high-rate electrochemical capacitor application. *J. Power Sources* **2014**, *272*, 1−7.
(39) Zhang, Z.; Jia, B.; Liu, L.; Zhao, Y.; Wu, H.; Qin, M.; Han, K.; Wang, W. A.; Xi, K.; Zhang, L.; Qi, G.; Qu, X.; Kumar, R. V. Hollow Multihole Carbon Bowls: A Stress-Release Structure Design for High-Stability and High-Volumetric-Capacity Potassium-Ion Batteries. *ACS Nano* **2019**, *13*, 11363−11371.
(40) Pei, F.; An, T.; Zang, J.; Zhao, X.; Fang, X.; Zheng, M.; Dong, Q.; Zheng, N. From Hollow Carbon Spheres to N-Doped Hollow Porous Carbon Bowls: Rational Design of Hollow Carbon Host for Li-S Batteries. *Adv. Energy Mater.* **2016**, *6*, 1502539.
(41) Zhang, Z.; Qin, M.; Jia, B.; Zhang, H.; Wu, H.; Qu, X. Facile synthesis of novel bowl-like hollow carbon spheres by the combination of hydrothermal carbonization and soft templating. *Chem. Commun.* **2017**, *53*, 2922−2925.
(42) Marechal, M.; Kortschot, R. J.; Demirörs, A. F.; Imhof, A.; Dijkstra, M. Phase behavior and structure of a new colloidal model system of bowl-shaped particles. *Nano Lett.* **2010**, *10*, 1907−1911.
(43) Zhang, X.; Zhao, R.; Wu, Q.; Li, W.; Shen, C.; Ni, L.; Yan, H.; Diao, G.; Chen, M. Ultrathin WS_2 nanosheets vertically embedded in a hollow mesoporous carbon framework − a triple-shell structure with enhanced lithium storage and electrocatalytic properties. *J. Mater. Chem. A* **2018**, *6*, 19004−19012.
(44) Chen, Y.; Xu, P.; Wu, M.; Meng, Q.; Chen, H.; Shu, Z.; Wang, J.; Zhang, L.; Li, Y.; Shi, J. Colloidal RBC-shaped, hydrophilic, and hollow mesoporous carbon nanocapsules for highly efficient biomedical engineering. *Adv. Mater.* **2014**, *26*, 4294−4301.
(45) Wang, D.; Wang, K.; Sun, L.; Wu, H.; Wang, J.; Zhao, Y.; Yan, L.; Luo, Y.; Jiang, K.; Li, Q.; Fan, S.; Li, J.; Wang, J. MnO_2 nanoparticles anchored on carbon nanotubes with hybrid supercapacitor-battery behavior for ultrafast lithium storage. *Carbon* **2018**, *139*, 145−155.
(46) Zhang, Y.; Huang, C.; Min, H.; Shu, H.; Gao, P.; Liang, Q.; Yang, X.; Liu, L.; Wang, X. Bowl-like double carbon layer architecture of hollow carbon@$FePO_4$@reduced graphene oxide composite as high-performance cathodes for sodium and lithium ion batteries. *J. Alloys Compd.* **2019**, *795*, 34−44.

https://dx.doi.org/10.1021/acssuschemeng.0c01835
ACS Sustainable Chem. Eng. 2020, 8, 10065−10072

(47) Qian, X.; Zhu, G.; Wang, K.; Zhang, F.; Liang, K.; Luo, W.; Yang, J. Bowl-like mesoporous polymer-induced interface growth of molybdenum disulfide for stable lithium storage. *Chem. Eng. J.* **2020**, *381*, 122651.
(48) Zhou, G.; Xu, X.; Yu, J.; Feng, B.; Zhang, Y.; Hu, J.; Zhou, Y. Vertically aligned MoS_2/MoOx heterojunction nanosheets for enhanced visible-light photocatalytic activity and photostability. *CrystEngComm* **2014**, *16*, 9025−9032.
(49) Chen, B.; Meng, Y.; He, F.; Liu, E.; Shi, C.; He, C.; Ma, L.; Li, Q.; Li, J.; Zhao, N. Thermal decomposition-reduced layer-by-layer nitrogen-doped graphene/MoS_2/nitrogen-doped graphene heterostructure for promising lithium-ion batteries. *Nano Energy* **2017**, *41*, 154−163.
(50) Xia, S.; Wang, Y.; Liu, Y.; Wu, C.; Wu, M.; Zhang, H. Ultrathin MoS_2 nanosheets tightly anchoring onto nitrogen-doped graphene for enhanced lithium storage properties. *Chem. Eng. J.* **2018**, *332*, 431−439.
(51) Yuan, G.; Wang, G.; Wang, H.; Bai, J. Half-cell and full-cell investigations of 3D hierarchical MoS_2/graphene composite on anode performance in lithium-ion batteries. *J. Alloys Compd.* **2016**, *660*, 62−72.
(52) Li, W.; Zhang, Z.; Zhang, W.; Zou, S. MoS_2 Nanosheets Supported on Hollow Carbon Spheres as Efficient Catalysts for Electrochemical Hydrogen Evolution Reaction. *ACS Omega* **2017**, *2*, 5087−5094.
(53) Wang, J.; Luo, C.; Gao, T.; Langrock, A.; Mignerey, A. C.; Wang, C. An advanced MoS_2 /carbon anode for high-performance sodium-ion batteries. *Small* **2015**, *11*, 473−481.
(54) Bai, Y.-L.; Liu, Y.-S.; Ma, C.; Wang, K.-X.; Chen, J.-S. Neuron-Inspired Design of High-Performance Electrode Materials for Sodium-Ion Batteries. *ACS Nano* **2018**, *12*, 11503−11510.
(55) Guo, B.; Yu, K.; Li, H.; Song, H.; Zhang, Y.; Lei, X.; Fu, H.; Tan, Y.; Zhu, Z. Hollow Structured Micro/Nano MoS_2 Spheres for High Electrocatalytic Activity Hydrogen Evolution Reaction. *ACS Appl. Mater. Interfaces* **2016**, *8*, 5517−5525.
(56) Xu, X.; Zhou, G.; Dong, X.; Hu, J. Interface Band Engineering Charge Transfer for 3D MoS_2 Photoanode to Boost Photoelectrochemical Water Splitting. *ACS Sustainable Chem. Eng.* **2017**, *5*, 3829−3836.
(57) Wang, L.; Xu, Z.; Wang, W.; Bai, X. Atomic mechanism of dynamic electrochemical lithiation processes of MoS_2 nanosheets. *J. Am. Chem. Soc.* **2014**, *136*, 6693−6697.
(58) Veerasubramani, G. K.; Park, M.-S.; Nagaraju, G.; Kim, D.-W. Unraveling the Na-ion storage performance of a vertically aligned interlayer-expanded two-dimensional MoS_2@C@MoS_2 heterostructure. *J. Mater. Chem. A* **2019**, *7*, 24557−24568.
(59) Li, H.; Yu, H.; Zhang, X.; Guo, G.; Hu, J.; Dong, A.; Yang, D. Bowl-like 3C-SiC Nanoshells Encapsulated in Hollow Graphitic Carbon Spheres for High-Rate Lithium-Ion Batteries. *Chem. Mater.* **2016**, *28*, 1179−1186.
(60) Zhang, S.; Wang, G.; Zhang, Z.; Wang, B.; Bai, J.; Wang, H. 3D Graphene Networks Encapsulated with Ultrathin SnS Nanosheets@Hollow Mesoporous Carbon Spheres Nanocomposite with Pseudocapacitance-Enhanced Lithium and Sodium Storage Kinetics. *Small* **2019**, *15*, 1900565.
(61) Zhang, K.; Park, M.; Zhou, L.; Lee, G.-H.; Li, W.; Kang, Y.-M.; Chen, J. Urchin-Like $CoSe_2$ as a High-Performance Anode Material for Sodium-Ion Batteries. *Adv. Funct. Mater.* **2016**, *26*, 6728−6735.
(62) Shao, M.; Cheng, Y.; Zhang, T.; Li, S.; Zhang, W.; Zheng, B.; Wu, J.; Xiong, W.-W.; Huo, F.; Lu, J. Designing MOFs-Derived FeS_2@Carbon Composites for High-Rate Sodium Ion Storage with Capacitive Contributions. *ACS Appl. Mater. Interfaces* **2018**, *10*, 33097−33104.
(63) Lukatskaya, M. R.; Dunn, B.; Gogotsi, Y. Multidimensional materials and device architectures for future hybrid energy storage. *Nat. Commun.* **2016**, *7*, 12647.
(64) Zhang, X.; Shen, C.; Wu, H.; Han, Y.; Wu, X.; Ding, W.; Ni, L.; Diao, G.; Chen, M. Filling few-layer ReS_2 in hollow mesoporous carbon spheres for boosted lithium/sodium storage properties. *Energy Storage Mater.* **2020**, *26*, 457−464.

https://dx.doi.org/10.1021/acssuschemeng.0c01835
ACS Sustainable Chem. Eng. 2020, 8, 10065−10072